Journal of Power Sources 195 (2010) 2909–2913

Contents lists available at ScienceDirect

Journal of Power Sources

journal homepage: www.elsevier.com/locate/jpowsour

Short communication

Surface modification of $LiNi_{0.5}Mn_{1.5}O_4$ by ZrP_2O_7 and ZrO_2 for lithium-ion batteries

H.M. Wu[a], I. Belharouak[a], A. Abouimrane[a], Y.-K. Sun[b], K. Amine[a,*]

[a] Chemical Sciences and Engineering Division, Argonne National Laboratory, 9700 South Cass Ave., Argonne, IL 60439, USA
[b] Department of Chemical Engineering, Center for Information and Communication Materials, Hanyang University, Seoul 133-791, South Korea

ARTICLE INFO

Article history:
Received 13 October 2009
Accepted 5 November 2009
Available online 14 November 2009

Keywords:
Lithium-ion batteries
$LiNi_{0.5}Mn_{1.5}O_4$
ZrO_2 coating
ZrP_2O_7 coating

ABSTRACT

The spinel $LiNi_{0.5}Mn_{1.5}O_4$ has been surface modified separately with 1.0 wt.% ZrO_2 and ZrP_2O_7 for the purpose of improving its cycle performance as a cathode in a 5-V lithium-ion cell. Although the modifications did not change the crystallographic structure of the surface-modified samples, they exhibited better cyclability at elevated temperature (55 °C) compared with pristine $LiNi_{0.5}Mn_{1.5}O_4$. The material that was surface modified with ZrO_2 gave the best cycling performance, only 4% loss of capacity after 150 cycles at 55 °C. Electrochemical impedance spectroscopy demonstrated that the improved performance of the ZrO_2-surface-modified $LiNi_{0.5}Mn_{1.5}O_4$ is due to a small decrease in the charge transfer resistance, indicating limited surface reactivity during cycling. Differential scanning calorimetry showed that the ZrO_2-modified $LiNi_{0.5}Mn_{1.5}O_4$ exhibits lower heat generation and higher onset reaction temperature compared to the pristine material. The excellent cycling and safety performance of the ZrO_2-modified $LiNi_{0.5}Mn_{1.5}O_4$ electrode was found to be due to the protective effect of homogeneous ZrO_2 nano-particles that form on the $LiNi_{0.5}Mn_{1.5}O_4$, as shown by transmission electron microscopy.

Published by Elsevier B.V.

1. Introduction

Great interest has arisen in use of $LiMn_2O_4$ spinels as cathode materials for lithium secondary batteries due to their high stability, low cost, abundance, nontoxicity, and outstanding power capability [1–3]. However, the poor cycling performance of the material at elevated temperature (50–80 °C) [4–6] has impeded its practical application. This poor cycling performance has been attributed largely to Mn dissolution from $LiMn_2O_4$ spinel particles into the $LiPF_6$-based electrolyte [4] due to the formation of HF resulting from the decomposition of the electrolyte. The dissolved Mn^{2+} is electrochemically reduced and is consequently deposited on the surface of the anode, which significantly deteriorates the cell performance [7].

The poor cycling behavior has been notably improved by two methods: first, substitution of a small fraction of cation (Li, Al, Mg, Ni, Co) for the Mn site [8–11] and anion (F, S) for the O site [12,13] in $LiMn_2O_4$; second, surface modification by use of a metal oxide and oxyfluoride coating on the $LiMn_2O_4$ particle [14–16]. The work on the substitution of the $LiMn_2O_4$ spinel has led to the discovery of many high-voltage cathode materials ($LiM_xMn_{2-x}O_4$, M = Cr, Co, Fe, Ni, Cu) [17–21]. The capacities and voltage plateaus in $Li/LiM_xMn_{2-x}O_4$ cells were found to be strongly dependent on the type of transition metals (M) and their content. Among those materials, $LiNi_{0.5}Mn_{1.5}O_4$ is of special interest due to its high discharge capacity of 140 mAh g^{-1} and attractive voltage plateau at around 4.7 V, which leads to increased energy density of the cell, although it was initially proposed as a 3-V cathode material [22]. In the ideal $LiNi_{0.5}Mn_{1.5}O_4$ spinel, the only redox species is Ni^{2+}, which oxidizes to Ni^{4+}, while Mn^{4+} ions do not participate in the redox reaction during cycling between 4 and 5 V. As expected, the electrochemically inactive Mn^{4+} leads to stable cycling performance of the $LiNi_{0.5}Mn_{1.5}O_4$ at room temperature. However, when cycled at elevated temperature (55 °C), the $LiNi_{0.5}Mn_{1.5}O_4$ undergoes severe capacity fade due to the high reactivity of the charged electrode with the electrolyte at high voltage.

In this study, we investigated the surface modification of $LiNi_{0.5}Mn_{1.5}O_4$ with ZrP_2O_7 or ZrO_2 additive for the purpose of limiting the surface reactivity between the charged $LiNi_{0.5}Mn_{1.5}O_4$ and the electrolyte at high voltage and high temperature.

2. Experimental

The sol–gel method was used to coat ZrP_2O_7 on the $LiNi_{0.5}Mn_{1.5}O_4$ [23] particles. First, H_3PO_4 (Sigma–Aldrich) was added to a $ZrOCl_2$ (Sigma–Aldrich) aqueous solution to form an acid zirconium phosphate gel, and then $LiNi_{0.5}Mn_{1.5}O_4$ powder was

* Corresponding author. Tel.: +1 6302522084; fax: +1 6309724451.
E-mail address: amine@anl.gov (K. Amine).

0378-7753/$ – see front matter. Published by Elsevier B.V.
doi:10.1016/j.jpowsour.2009.11.029

added into the gel and stirred for 4 h. After filtration, the resulting powder was heated at 400 °C for 6 h in air.

For the ZrO_2 coating, $ZrCl_4$ (Sigma–Aldrich) was first dissolved in ether (Sigma–Aldrich); subsequently, $LiNi_{0.5}Mn_{1.5}O_4$ (insoluble in ether) was suspended in the solution for 30 min in air. During this process, ether-soluble $ZrCl_4$ was converted to insoluble ZrO_2, which deposited on the surface of the $LiNi_{0.5}Mn_{1.5}O_4$ powder. The remaining solvent was vacuum removed, and the powder was calcined at 400 °C for 6 h. In both cases, the ZrP_2O_7 and ZrO_2 coating amount was about 1.0 wt.%.

Powder X-ray diffraction (Siemens D5000 diffractometer) was used to determine the crystal structure and the phase composition of the samples. The radiation source was Cu Kα. The samples were scanned from $2\theta = 10$–80° at a scan rate of 5 s per 0.02°. The surface of the samples was characterized by transmission electron microscopy (TEM, JEOL 2010).

Differential scanning calorimetry (DSC) was conducted on electrochemically delithiated electrodes by analysis with a Perkin-Elmer Pyris-1 instrument. Typically, 3 mg of scraped electrode material and 3 μl of electrolyte were hermetically sealed inside stainless-steel high-pressure capsules to prevent leakage of the pressurized solvents. The DSC curves were recorded between room temperature and 375 °C at a scan rate of 10 °C min^{-1}. An empty stainless-steel capsule was used as a reference pan. To ensure reproducibility, at least two heat measurements were conducted for each temperature.

The electrochemical characteristics of the electrodes were determined in tests with CR2032 coin-type cells. The cathodes were prepared by casting a slurry of 80 wt.% active oxide materials, 10 wt.% carbon black, and 10 wt.% polyvinylidene fluoride dispersed in *N*-methyl-2-pyrrolidone on aluminum foil. The electrodes were dried completely under vacuum at 75 °C for 24 h. In these tests, the mass of active materials in the cathodes was about 8 mg (1.6 cm^2). Both pristine and surface-modified $LiNi_{0.5}Mn_{1.5}O_4$ materials were tested as the cathode. Lithium metal was used as the anode. The separator was porous polypropylene film (Celgard 2325). The electrolyte was 1.2 M $LiPF_6$ in ethylene carbonate-ethyl methyl carbonate (3:7 by weight). The coin cells were assembled in a dry Ar-filled glove box. Electrochemical measurements were conducted with a Maccor Series 4000 battery cycler. Electrochemical impedance spectroscopy (EIS) was conducted in a frequency range from 1 MHz to 0.01 Hz, using an ac signal with 5 mV amplitude on an IM6 electrochemical impedance analyzer.

3. Results and discussion

Fig. 1 shows the X-ray diffraction (XRD) patterns of (a) pristine $LiNi_{0.5}Mn_{1.5}O_4$, (b) ZrP_2O_7-surface-modified $LiNi_{0.5}Mn_{1.5}O_4$, and (c) ZrO_2-surface-modified $LiNi_{0.5}Mn_{1.5}O_4$. The three samples present a similar cubic spinel structure with *Fd*-3*m* space group, in which lithium ions occupy the tetrahedral (8*a*) sites and the transition metal ions (Mn and Ni) statistically reside at the octahedral (16*d*) site. The diffraction peaks are extremely narrow, indicating high crystallinity. The NiO diffraction peaks are negligible. The finding of no diffraction pattern corresponding to the coating material was expected since the amount of coating material is very small (about 1.0 wt.%).

Fig. 2 shows a scanning electron microscopy image of the pristine $LiNi_{0.5}Mn_{0.5}O_4$ powder. The material is made of 5–10 μm spherical secondary particles, which are suitable for surface coating and modification. These secondary particles are made of crystalline and rectangular submicron primary particles. The tap density of this material is very high, 2 g cm^{-3}, because of the highly dense and aggregated primary particles. As a result, one can expect a high degree of cathode powder loading in the electrode and, therefore, high volumetric energy density at the cell level.

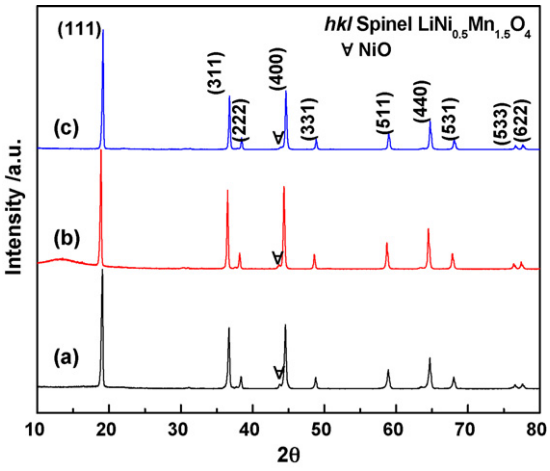

Fig. 1. Powder XRD patterns of (a) pristine $LiNi_{0.5}Mn_{1.5}O_4$, (b) ZrP_2O_7-coated $LiNi_{0.5}Mn_{1.5}O_4$, and (c) ZrO_2-coated $LiNi_{0.5}Mn_{1.5}O_4$.

Fig. 3 shows high-resolution TEM images of the pristine (Fig. 3a), ZrP_2O_7-modified $LiNi_{0.5}Mn_{1.5}O_4$ particles (Fig. 3b), and ZrO_2-modified $LiNi_{0.5}Mn_{1.5}O_4$ particles (Fig. 3c–e). The ZrP_2O_7-modified material shows a large and isolated conglomeration of ZrP_2O_7 particles on the surface of the high-voltage cathode material. This conglomeration had an amorphous structure, as shown by the electron diffraction pattern in Fig. 3b inset. In contrast, ZrO_2-modified material shows highly uniform and dense nano-particles of ZrO_2 on the surface (Fig. 3d). In this case, the nano-particles are highly crystalline, with an average particle size of 10 nm (Fig. 3e). The high uniformity of the ZrO_2 coating is probably caused by the slow heat treatment, which results in the formation of $Zr(OH)_4$ at the cathode material surface from the reaction of ether-dissolved $ZrCl_4$ salt with air moisture as reported by others [24]. After the heat treatment, $Zr(OH)_4$ is transformed to ZrO_2 nano-particles on the electrode material surface. From the TEM images, the ZrO_2 nano-particles are densely dispersed on the surface of the cathode and do not form a complete coating, which may not impede the lithium diffusion during cycling while protecting the surface of the material.

Fig. 4 shows the initial charge and discharge voltage profiles of coin cells with pristine, ZrP_2O_7-coated, and ZrO_2-coated $LiNi_{0.5}Mn_{1.5}O_4$ as the cathode (lithium metal anode). The cells were cycled at a current density of 120 mA g^{-1} between 3.2 V and 4.95 V. All the cells have a flat voltage plateau at 4.7 V which correspond to the Ni^{2+}/Ni^{4+} redox process, and also have a very small voltage region at 4.0 V which correspond to Mn^{3+}/Mn^{4+} redox process. The initial capacities of the ZrP_2O_7-coated and ZrO_2-coated

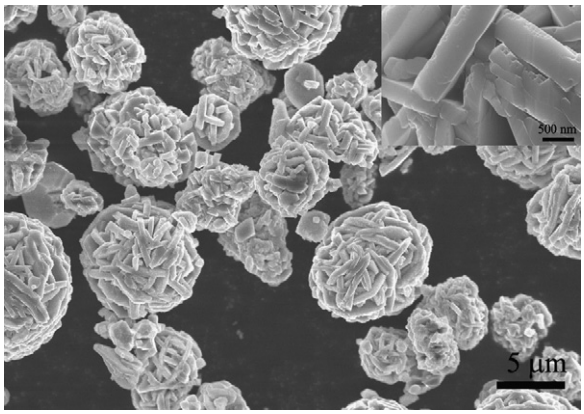

Fig. 2. SEM image of pristine $LiNi_{0.5}Mn_{1.5}O_4$.

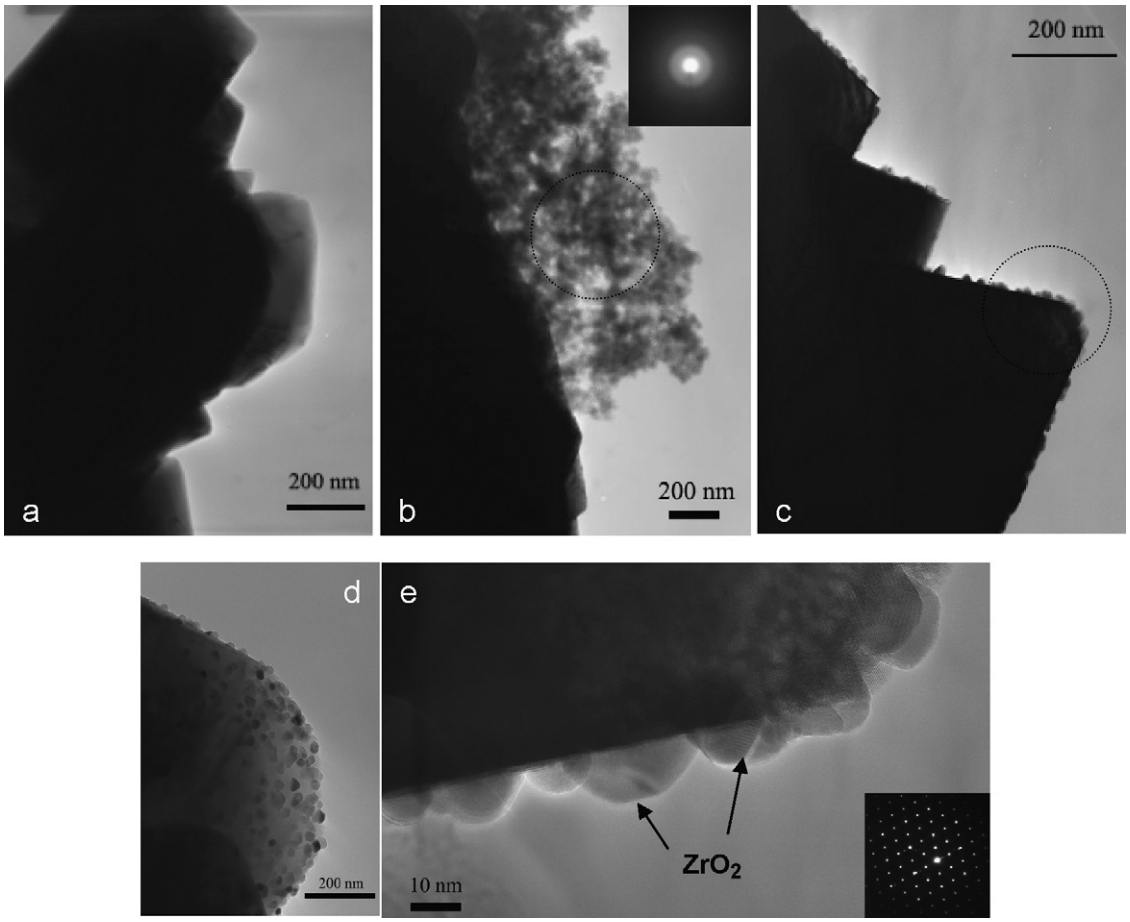

Fig. 3. TEM images of (a) pristine $LiNi_{0.5}Mn_{1.5}O_4$, (b) ZrP_2O_7-coated $LiNi_{0.5}Mn_{1.5}O_4$, and (c–e) ZrO_2-coated $LiNi_{0.5}Mn_{1.5}O_4$.

$LiNi_{0.5}Mn_{1.5}O_4$ electrodes were 120 and 118 mAh g^{-1}, respectively. Because the coating amount in both cases is very small, the effect on the initial cell capacity was negligible when compared to that of the non-coated material (123 mAh g^{-1}).

Fig. 5 shows the cycling performance of cells based on lithium metal as the anode and pristine, ZrP_2O_7-coated, and ZrO_2-coated $LiNi_{0.5}Mn_{1.5}O_4$ as the cathode. Cell cycling was carried out at 25 °C for 50 cycles and 55 °C for 150 cycles. At 25 °C, both coated and non-coated samples exhibited excellent cycle stability with no capacity fade after 50 cycles. However, at 55 °C, the cells with the non-coated and the ZrP_2O_7-coated cathodes exhibited 27% and 20% capacity fade after 150 cycles, respectively. In the non-coated cathode cell, the poor cycling performance was caused by the high surface reactivity of the Ni^{4+} from the charged cathode with the electrolyte. This reaction was accelerated with the increase in the cycling temperature. As shown in Fig. 3b, the ZrP_2O_7-modified material shows scattered and aggregated particles at the surface of the high-voltage cathode, resulting in limited protection against surface reactivity, especially during high-temperature cycling. The ZrO_2-coated material, on the other hand, shows outstanding cyclability with less than 4% capacity fade after 150 cycles. This result is due to the good surface protection from the uniform and highly dense ZrO_2 particles at the cathode surface (Fig. 3e), which play a role in suppressing the surface reactivity between the charged electrode and the electrolyte.

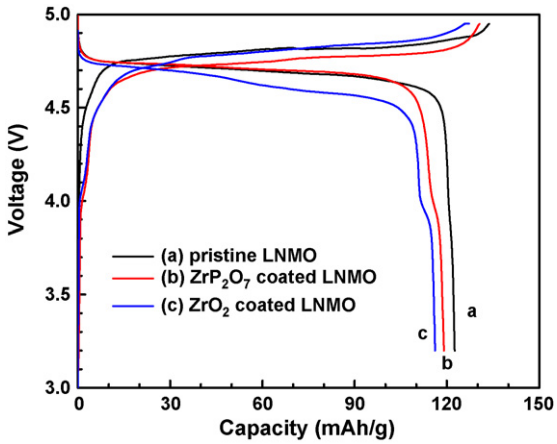

Fig. 4. First charge and discharge curves of (a) pristine $LiNi_{0.5}Mn_{1.5}O_4$, (b) ZrP_2O_7-coated $LiNi_{0.5}Mn_{1.5}O_4$, and (c) ZrO_2-coated $LiNi_{0.5}Mn_{1.5}O_4$. Note that LNMO = $LiNi_{0.5}Mn_{1.5}O_4$.

To better understand the superior cycling stability at 55 °C of the ZrO_2-coated $LiNi_{0.5}Mn_{1.5}O_4$ compared to the non-coated or ZrP_2O_7-coated $LiNi_{0.5}Mn_{1.5}O_4$, we performed AC impendence studies of the cells after 5 and 100 cycles. The cells were cycled at 55 °C and rested for 1 h at room temperature before the AC impedance measurements. Fig. 6 shows the EIS plots obtained for pristine, ZrP_2O_7-coated, and ZrO_2-coated $LiNi_{0.5}Mn_{1.5}O_4$. These Nyquist plots were fitted using the equivalent circuit shown in Fig. 6c and the fitting parameters are reported in Table 1. According to the literature [25], R_e represents the solution resistance; R_{sf} and CPE_1 signify the diffusion resistance of Li^+ ions through the solid-electrolyte interface (SEI) layer and the corresponding constant phase element (CPE); R_{ct} and CPE_2 correspond to the charge transfer resistance and the corresponding CPE, while R_w (not cal-

Table 1
Fitting results of Nyquist plots using the equivalent circuit of pristine, ZrP_2O_7-coated, and ZrO_2-coated $LiNi_{0.5}Mn_{1.5}O_4$ using the equivalent circuit in Fig. 6c.

	R_e (Ω)		R_{sf} (Ω)		R_{ct} (Ω)	
	5[a]	100[a]	5[a]	100[a]	5[a]	100[a]
Pristine $LiNi_{0.5}Mn_{1.5}O_4$	1.647	1.449	16.41	8.124	52.9	107.5
ZrP_2O_7-coated $LiNi_{0.5}Mn_{1.5}O_4$	1.622	1.334	63.43	9.964	34.12	77.08
ZrO_2-coated $LiNi_{0.5}Mn_{1.5}O_4$	2.296	1.372	73.48	10.43	51.37	4.14

[a] Cycle number.

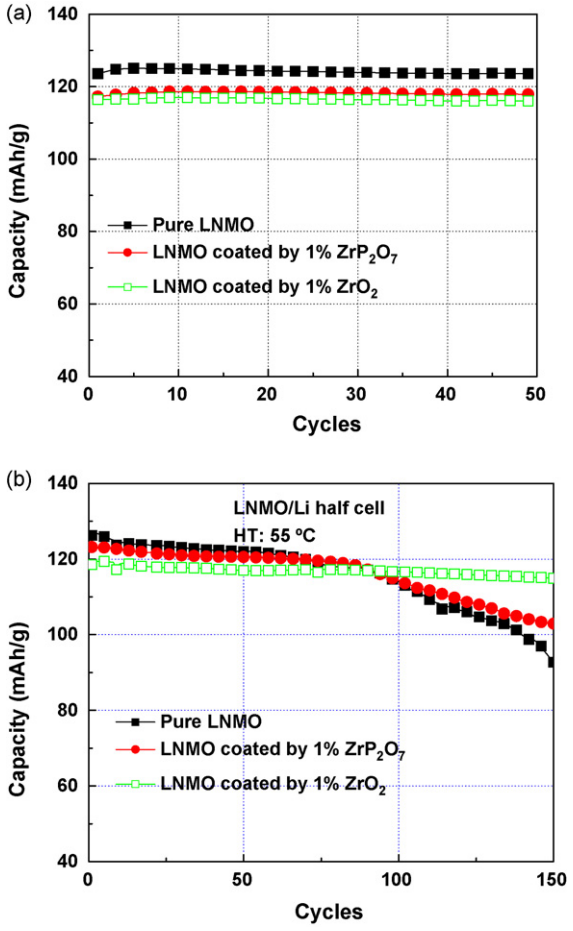

Fig. 5. Cycle stability of pristine $LiNi_{0.5}Mn_{1.5}O_4$, ZrP_2O_7-coated $LiNi_{0.5}Mn_{1.5}O_4$, and ZrO_2-coated $LiNi_{0.5}Mn_{1.5}O_4$ at (a) room temperature and (b) high temperature (55 °C). Note that LNMO = $LiNi_{0.5}Mn_{1.5}O_4$.

culated here) is related to the solid-state diffusion of Li^+ ions in the active materials corresponding to the slope of the line at low frequency. For these three samples, the results indicate that the R_e values slightly changed whereas R_{sf} resistance decreased to close values after cycling. In the case of ZrP_2O_7-coated $LiNi_{0.5}Mn_{1.5}O_4$ samples, the R_{ct} resistance increased significantly after 100 cycles: from 52.9 Ω to 107.5 Ω, and from 34.2 Ω to 77.08 Ω, respectively. The significant increases in R_{ct} are likely due to the side reactions of the oxidation of the electrolyte at the SEI interface during cycling. In contrast, the R_{ct} resistance of the ZrO_2-coated $LiNi_{0.5}Mn_{1.5}O_4$ electrode significantly decreased from 51.37 Ω to 4.14 Ω after 100 cycles. This result clearly attests to the improvement of the charge transfer phenomenon at the interface of the electrode that was protected with highly dense nano-sized ZrO_2 particles against the occurrence of side reactions at high voltage and high temperature. Therefore, the overall electrochemical properties of the ZrO_2-coated $LiNi_{0.5}Mn_{1.5}O_4$ electrode were much improved and very stable cycling was observed at high temperature.

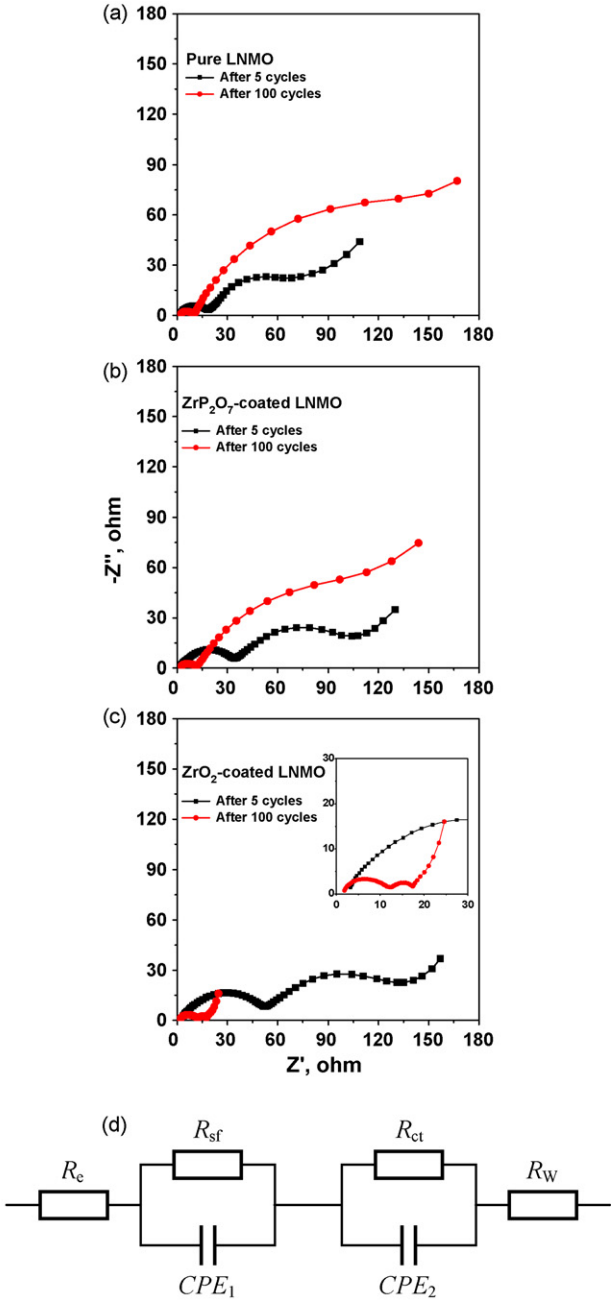

Fig. 6. EIS results of (a) pristine $LiNi_{0.5}Mn_{1.5}O_4$, (b) ZrP_2O_7-coated $LiNi_{0.5}Mn_{1.5}O_4$, and (c) ZrO_2-coated $LiNi_{0.5}Mn_{1.5}O_4$ after 5 cycles and 100 cycles; (d) the corresponding equivalent circuit. Note that LNMO = $LiNi_{0.5}Mn_{1.5}O_4$; other abbreviations defined in text.

Fig. 7 shows DSC profiles of pristine $LiNi_{0.5}Mn_{1.5}O_4$, ZrP_2O_7-coated $LiNi_{0.5}Mn_{1.5}O_4$, and ZrO_2-coated $LiNi_{0.5}Mn_{1.5}O_4$ electrodes, which had been charged to 4.95 V. Compared with the pristine material, the ZrP_2O_7-coated $LiNi_{0.5}Mn_{1.5}O_4$ shows a slight

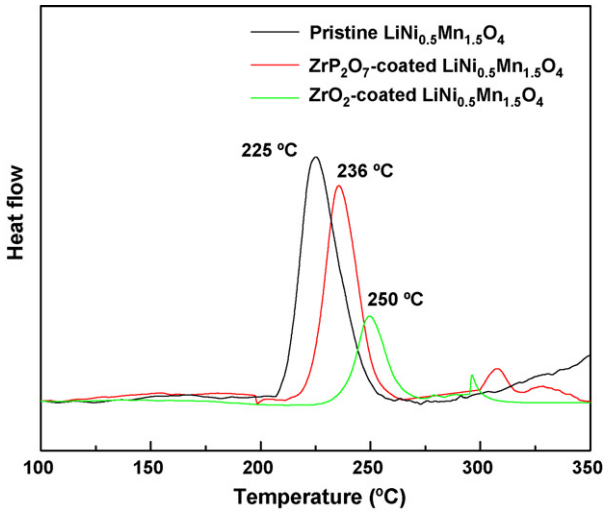

Fig. 7. DSC profiles of pristine $LiNi_{0.5}Mn_{1.5}O_4$, ZrP_2O_7-coated $LiNi_{0.5}Mn_{1.5}O_4$, and ZrO_2-coated $LiNi_{0.5}Mn_{1.5}O_4$.

improvement in safety performance with a slight increase in the onset temperature of reaction with the electrolyte from 210 °C to 215 °C and a decrease in the heat generation from 532 J g^{-1} to 396 J g^{-1}. In the case of the ZrO_2-coated $LiNi_{0.5}Mn_{1.5}O_4$, a clear increase in the onset temperature of reaction from 210 °C to 230 °C was observed, which is probably due to the decrease of the reactivity because of the protection by highly dense ZrO_2 coating. The material also shows a significant drop in the heat generation (139 J g^{-1}) when compared to the non-coated and ZrP_2O_7-coated material.

4. Conclusion

Spinel $LiNi_{0.5}Mn_{1.5}O_4$ particles were modified by coating their surface with ZrO_2 or ZrP_2O_7. Coin cells with the ZrO_2-coated $LiNi_{0.5}Mn_{1.5}O_4$ cathode showed remarkable improvement in cycling stability, with capacity retention of 96% after 150 cycles at 55 °C, whereas the pristine and ZrP_2O_7-coated $LiNi_{0.5}Mn_{1.5}O_4$ cathodes exhibited a capacity retention of only 73% and 80%, respectively, after the same cycling period. The DSC analysis indicated that the coating also improved the thermal stability significantly. These excellent properties might have originated from the suppression of the interfacial resistance increase between cathode and electrolyte by protecting the cathode against surface electrolyte reactivity with formation of homogeneous and dense nano-particles of ZrO_2.

References

[1] J.-M. Tarascon, D. Guyomard, J. Electrochem. Soc. 138 (1991) 2865.
[2] G. Pistoia, G. Wang, Solid State Ionics 66 (1993) 135.
[3] A. Yamada, M. Tanaka, Mater. Res. Bull. 30 (1995) 715.
[4] D.H. Jang, Y.J. Shin, S.M. Oh, J. Electrochem. Soc. 143 (1996) 2204.
[5] Y. Gao, J. Dahn, J. Electrochem. Soc. 143 (1996) 1783.
[6] A. Blyr, C. Sigala, G.G. Amatucci, D. Guyomard, Y. Chabre, J.-M. Tarascon, J. Electrochem. Soc. 145 (1998) 194.
[7] S. Komaba, N. Kumagai, Y. Kataoka, Electrochim. Acta 47 (2002) 1229.
[8] J.M. Tarascon, U.S. Patent 5,425,932 (1995).
[9] J.M. Tarascon, W. McKinnon, F. Coowar, T. Bowmer, G. Amatucci, D. Guyomard, J. Electrochem. Soc. 141 (1994) 1421.
[10] Robertson, W. Howard, J. Electrochem. Soc. 144 (1997) 3505.
[11] J.H. Lee, J.K. Hong, D.H. Jang, Y.K. Sun, S.M. Oh, J. Power Sources 89 (2000) 7.
[12] Y.-K. Sun, Y.-S. Jeon, H.-J. Lee, Electrochem. Solid-State Lett. 3 (2000) 7.
[13] G.G. Amatucci, N. Pereira, T. Zheng, J.-M. Tarascon, J. Electrochem. Soc. 148 (2001) A171.
[14] J.S. Gnanaraj, V.G. Pol, A. Gedanken, D. Aurbach, Electrochem. Commun. 5 (2003) 940.
[15] J.-M. Han, S.-T. Myung, Y.-K. Sun, J. Electrochem. Soc. 153 (2006) A1290.
[16] K.-S. Lee, S.-T. Myung, K. Amine, H. Yashiro, Y.-K. Sun, J. Mater. Chem. 19 (2009) 1995.
[17] K. Amine, J. Liu, S. Kang, I. Belharouak, Y. Hyung, D. Vissers, G. Henriksen, J. Power Sources 129 (2004) 14.
[18] K. Amine, H. Tukamoto, H. Yasuda, Y. Fujita, J. Power Sources 68 (1997) 604.
[19] Q. Zhong, A. Bonakdarpour, M. Zhang, Y. Gao, J.R. Dahn, J. Electrochem. Soc. 144 (1997) 205.
[20] C. Sigala, A. Le Gal La Salle, Y. Piffard, D. Guyomard, J. Electrochem. Soc. 148 (2001) A812.
[21] H. Kawai, M. Nagata, H. Tukamoto, A.R. West, J. Mater. Chem. 8 (1998) 837.
[22] K. Amine, H. Tukamoto, H. Yasuda, Y. Fujita, J. Electrochem. Soc. 143 (1996) 1607.
[23] H.M. Wu, I. Belharouak, H. Deng, A. Abouimrane, Y.K. Sun, K. Amine, J. Electrochem. Soc 156 (2009) A1047.
[24] S. Licht, H. Wu, X. Yu, Y. Wang, Chem. Commun. (2008) 3257.
[25] J. Xie, X.B. Zhao, G.S. Cao, M.J. Zhao, S.F. Su, J. Power Sources 140 (2) (2005) 350.